Fast Dynamics of Floating Triple Lines

X. Noblin, A. Buguin, and F. Brochard-Wyart*

Institut Curie, PCC-UMR 168, 11 rue Pierre et Marie Curie, 75231 Paris Cedex 05, France

We study the contour (or contact) line of a large water puddle floating on an organic liquid substrate. The line tension $\mathcal{T}$ is a two-dimensional analogue of surface tension. We manipulate the line through a vertical metallic rod. (i) When stretched by a horizontal force f, the line makes a kink characterized by an angle 2θ ($f = 2\mathcal{T}\cos\theta$), which allows us to measure $\mathcal{T}$. (ii) Moved sinusoidally, we generate "triplons" of wavevectors q along the line. In the gravity regime ($q\kappa^{-1} < 1$, where κ^{-1} is the capillary length), the measured dispersion relation is $\omega(q) \simeq q^{1.51\pm0.05}$. An improved version of our previous dynamical model gives an exponent 3/2.

1. Introduction

The statics and dynamics of contact lines between a solid, a liquid, and air, in partial wetting conditions (finite contact angle), have been extensively studied, both theoretically[1–6] and experimentally.[7–13] The line elasticity (first constructed in ref 1) is anomalous. If the line undulates in space with amplitude u_q for a wave vector q, the energy is of the form (for small equilibrium contact angles θ_E):

$$E_{el} = \frac{1}{2}\gamma\theta_E^2\sum_q |q|u_q^2 \qquad (1)$$

in the capillary regime ($q > \kappa = \sqrt{(\rho g)/\gamma}$) (where γ is the liquid surface tension, ρ the density, and g the gravitational acceleration). The q factor in eq 1 comes from distortions of the liquid–gas interface, giving energies $\propto q^2$, which have to be integrated (in the direction normal to the line) up to the penetration length ($\sim q^{-1}$). This elasticity, which cannot be described in terms of a line tension (which gives $E_{el} \propto q^2$), has been named "fringe elasticity" by P. G. de Gennes.[3] The deformation of the contact line pinned on a single defect, calculated with the fringe elasticity (1), decreases logarithmically with distance x from the defect measured along the unperturbed line.[4] Experimental studies have confirmed these predictions.[10]

The dynamics of line fluctuations, described by the fringe elasticity, have been studied in both viscous[4–7] and inertial[6–8,12–13] regimes:

(a) In the *viscous regime*, the dissipation occurs mostly in the liquid wedge. The dispersion relation can be deduced from a transfer of elastic energy into viscous dissipation. If η is the liquid viscosity, one gets

$$\frac{dE_{el}}{dt} + \frac{\eta}{\theta_E}\dot{u}^2 \ln = 0 \qquad (2)$$

where $\ln = \ln(\kappa^{-1}/a) \simeq 10–20$ is a logarithmic factor describing the divergence of the viscous dissipation in a liquid wedge, which involves two cut offs: κ^{-1} at large scales and a molecular length a at short distances.[2] For a mode $u = u_q e^{iqx}e^{-t/\tau_q}$, this balance leads to $\gamma\theta_E^2|q| = \eta/\theta_E\tau_q \ln$ or

$$\frac{1}{\tau_q} = \frac{\gamma\theta_E^3}{\eta \ln}|q| = c|q| \qquad (3)$$

with $c = \gamma\theta_E^3/(\eta \ln)$. Experimentally, a modulation of the contact line has been produced by the deposition of a row of small equidistant droplets.[7,8] A liquid front is pushed until it comes into contact with the droplets. The relaxation of the line is in good agreement with eq 3. In these experiments, the main difficulty is to obtain model substrates, with a very small contact angle hysteresis. Even on silanized silicon wafers, only modulations of large q vectors can be observed. For low q, the elastic energy is weak, and pinning by chemical defects blocks the line motion.

(b) In the *inertial regime*, the mechanical energy is conserved and the modes are propagative.[4] Writing $u = u_q e^{iqx}e^{i\omega t}$, the balance of fringe elasticity and kinetic energy gives

$$\frac{1}{2}\gamma\theta_E^2|q|u_q^2 = M\omega^2 u_q^2 \qquad (4)$$

M is the mass of liquid put into motion by the line fluctuations in a region of volume $q^{-2}\theta_E$ (by unit length of the line). With $M = \rho q^{-2}\theta_E$, eq 4 leads to

$$\omega^2 = \theta_E\frac{\gamma}{\rho}q^3 \qquad (5)$$

These inertial line fluctuations, named triplons, have been studied with superfluid ⁴He. ⁴He does not wet cesium, but the large contact angle hysteresis has prevented any observations.[12] Recently, the conditions of pseudo partial wetting of ⁴He on silicon wafers have allowed Poujade et al.[13] to observe the triplons and to confirm the dispersion relation (eq 5).

This fringe elasticity holds in the capillary regime corresponding to large wave vectors. Our aim here is to study the opposite limit of small wave vectors ($q < \kappa$), where gravity becomes important. Because the surface deformations are cut off at a distance κ^{-1}, the elastic energy

* To whom correspondence should be adressed. E-mail: brochard@curie.fr.

(1) Joanny, J. F.; de Gennes, P. G. *J. Chem. Phys.* **1984**, *81*, 552.
(2) de Gennes, P. G. *Rev. Mod. Phys.* **1985**, *57*, 827.
(3) de Gennes, P. G.; Brochard, F.; Quéré, D. Gouttes, bulles, perles et ondes, Ed.; Belin, 2002.
(4) de Gennes, P. G. *C. R. Acad. Sci. Paris* **1986**, *11*, 302.
(5) Brochard-Wyart, F.; de Gennes, P. G. *Langmuir* **1991**, *7*, 3216.
(6) Brochard, F. *J. Phys. II Fr.* **1993**, *3*, 21–26.
(7) Ondarçuhu, T.; Veyssié, M. *Nature* **1991**, 352.
(8) Ondarçuhu, T. *Mod. Phys. Lett. B* **1992**, *6* (15), 901–916.
(9) Nadkarni, G. D.; Garoff, S. *Europhys. Lett.* **1992**, *20*, 523–528.

(10) Marsh, J. A.; Cazabat, A. M. *Phys. Rev. Lett.* **1993**, *71*, 2433–2436.
(11) Paterson, A. *Ann. Phys. Fr.* **1996**, *21*, 337.
(12) Prevost, A.; Poujade, M.; Rolley, E.; Guthmann, C. *Physica B* **2000**, *280*, 80.
(13) Poujade, M.; Guthmann, C.; Rolley, E. To be published.

of long wavelength modulations of the contact line returns to a standard form[5]

$$E_{\text{el}} = \sum_q \frac{1}{2} \mathcal{T} q^2 u_q^2 \qquad (6)$$

where $\mathcal{T}$ is an effective line tension (calculated in the next section).

$\mathcal{T}$ is the 2D analogue of interfacial energy between liquid/air or liquid A/liquid B, as first pointed by I. Langmuir. The thickness of large liquid puddles, flattened by gravity, is

$$e_c = 2\kappa^{-1} \sin\left(\frac{\theta_E}{2}\right) \qquad (7)$$

The liquid film of thickness e_c coexists with the dry solid substrate. $\mathcal{T}$ corresponds to the border energy between the dry and the wet solid. The capillarity in 3D can be transposed: minimal surfaces become minimal lines bordering the liquid puddles. However, these minimal lines are not easy to observe on solid substrates: chemical heterogeneities and surface roughness pin the line on defects at many scales.

But all these phenomena can easily be observed on liquid substrate! The liquid substrate is free of hysteresis. Moreover, for the dynamics, the viscous dissipation on a liquid substrate is reduced: inertial regimes show up more frequently. We study here water puddles floating on carbon tetrachloride (CCl_4).

Nevertheless, the use of liquid substrate does give further complications: (a) deformations of the CCl_4 free surface and (b) flows induced by the water inside CCl_4. This explains why this configuration has been poorly studied[16–18] since the famous paper of Langmuir in 1933.[14]

In this article, we focus on the statics and dynamics of the collective modes of the triple lines (triplons).

In section 2, we compute the line tension and also show evidence for the presence of a 2D Laplace pressure. We measure $\mathcal{T}$ directly by stretching the line with a force f.

In section 3, we drive the line with a metallic rod at a frequency ω and we observe the propagation of the sinusoidal deformations of wave vector q. The dispersion relation is also interpreted theoretically.

2. Statics of Floating Triple Lines

2.1. Floating Puddles. The liquid A (water) is non-miscible and does not wet the heavier liquid substrate B. The spreading coefficient $S = \gamma_B - (\gamma_{AB} + \gamma_A)$ is negative (γ_{ij} are respectively the B/air, A/B, and A/air interfacial tensions). On this substrate, a small water drop forms a lens, composed of two spherical caps. The Neumann construction satisfies $\gamma_B + \gamma_{AB} + \gamma_A = 0$. A large drop is flattened by gravity and forms a thick (millimetric) sheet of water floating on the B liquid bath. The covered liquid is characterized by the following parameters:

(a) Effective Surface Tension $\tilde{\gamma}_B$. The energy of a floating film of thickness e can be written as

$$F = \left[\gamma_{AB} + \gamma_A + \frac{1}{2}\tilde{\rho}ge^2\right]\mathcal{A} \qquad (8)$$

where $\tilde{\rho}$ is the density of liquid A corrected by Archimedian

(14) Langmuir, I. *J. Chem. Phys* **1933**, *1*, 756.
(15) Fermigier, M.; Paterson, A. *Phys. Fluids* **1997**, *9*, 2210.
(16) Joanny, J. F. *Phys. Chem. Hydrodyn.* **1987**, *3* (9), 183.
(17) Fraaije, J. G. E.; Cazabat, A. M. *J. Colloid Interface Sci.* **1989**, *133*, 452−460.
(18) Brochard-Wyart, F.; Martin, P.; Redon, C. *Langmuir* **1993**, *9*, 3682−3690.
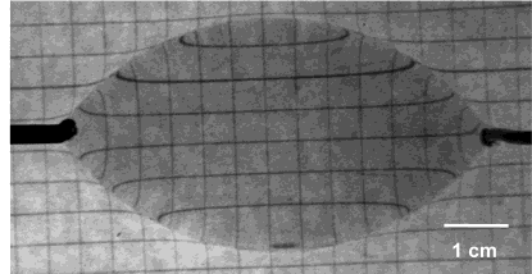
Figure 1. Minimal lines: arcs of circles formed by a large water drop laying on CCl_4 when stretched by opposite forces.

forces, $\tilde{\rho} = \rho_A/\rho_B(\rho_B - \rho_A)$,[14] and $\mathcal{A}$ is the surface of the film. The effective surface tension of the coated B liquid is $\tilde{\gamma}_B = \partial F/\partial \mathcal{A}|_{\mathcal{A}e=cst}$. This leads to

$$\tilde{\gamma}_B = \left[\gamma_{AB} + \gamma_A - \frac{1}{2}\tilde{\rho}ge^2\right] \qquad (9)$$

(b) Coexistence between Coated/Bare Substrate. The coexistence between the bare substrate and the floating film implies $\tilde{\gamma}_B = \gamma_B$. This equality defines the equilibrium thickness e_c of the film

$$\frac{1}{2}\tilde{\rho}ge_c^2 = |S| \qquad (10)$$

For CCl_4/H_2O, one gets $e_c = 7.1$ mm.

(c) Surface Pressure Π_A. The concept of surface pressure was introduced by Langmuir for monolayers of insoluble surfactants deposited on water.[14] It applies in fact to all kinds of liquid surface coatings, which are tensioactive, that is, which modify the liquid surface tension. In our case, the surface tension of the coated film is $\tilde{\gamma}_B$. By definition, the surface pressure of the A film is $\Pi_A = \gamma_B - \tilde{\gamma}_B$. In term of the film thickness, using eqs 9 and 10 we obtain

$$\Pi_A = \frac{1}{2}\tilde{\rho}g(e^2 - e_c^2) \qquad (11)$$

(d) Triple Line Tension. The boundary between the two coexisting states (bare, coated B bath), called the triple line or contact line, costs an energy $\mathcal{T}$ per unit length. This line tension is macroscopic (of order $\gamma\kappa^{-1}$) and masks the intrinsic line tension[3,19] of order γa, where a is a molecular size. $\mathcal{T}$ plays in 2D a role similar to that of the surface tension in 3D. This energy tends to minimize the length of the line. Lines make minimal curves, as surfaces in 3D make minimal surfaces (like spheres, hyperboloids, ...). We show in Figure 1 a large flat drop, initially circular, stretched by two opposite forces applied at both ends. The contour is composed of two arcs of circles.

(e) 2D Laplace Law. The Laplace law relates the hydrostatic pressure to the curvature of interfaces, which tend to minimize their area. By analogy, we can write a 2D Laplace law, which links the curvature of the line to the difference in surface pressures. A large drop of water has a circular shape of radius R. We can make a transformation $R \rightarrow R + dR$ (radial dilatation of the flat drop), which increases the surface by $2\pi R\,dR$ and the contour by $2\pi\,dR$. If Π_A and Π_B are the surface pressures inside and outside the drop, the surface work is $2\pi R\,dR(\Pi_B - \Pi_A)$ and the line work is $2\pi\mathcal{T}\,dR$. At equilibrium, the total work cancels. We obtain the analogous Laplace law for 2D, which can be formalized to any form of contour:

(19) Dussaud, A.; Vignes-Adler, M. *Langmuir* **1997**, *13*, 587−589.

$$\Pi_A - \Pi_B = \frac{\mathcal{T}}{\mathcal{R}} \tag{12}$$

where $\mathcal{R}$ is the local curvature of the line. It can be positive or negative. For our case, $\Pi_B = 0$ outside the drop at equilibrium. Equations 11 and 12 show that smaller droplets are slightly thicker. More precisely, it is possible to derive the thickness versus the radius R of the puddle:

$$\frac{1}{2}\tilde{\rho}ge^2 = \frac{1}{2}\tilde{\rho}ge_c^2 + \frac{\mathcal{T}}{R} \tag{13}$$

(f) Puddles Distortions: Minimal Curves. If one pulls on a particular point of a guitar string, it takes the shape of a triangle. Each part has zero curvature. The problem is not exactly the same for a puddle. If R is much larger than κ^{-1}, any macroscopic deformation must keep the surface area of the A wet region constant. This restriction is embodied in a Lagrange multiplier in the expression of the energy of the drop, which is the 2D pressure. Any contour which minimizes the energy obeys eq 12.

We present here a simple application of the 2D Laplace law. A circular flat drop is pulled with equal strength f on two opposite points. The Laplace 2D law ($\Pi_A = \mathcal{T}/\mathcal{R}$) forces the radius of curvature to be constant. The equilibrium shape is made of two circular arcs, with an angle 2θ given by force balance: $f = 2\mathcal{T}\cos\theta$. If we stretch the drop on four points, we can obtain four arcs of a circle with a negative curvature.

2.2. Line Tension $\mathcal{T}$. *(a) Derivation of $\mathcal{T}$.* The goal here is to derive the line tension $\mathcal{T}$. $\mathcal{T}$ is calculated in ref 14 by a delicate balance of forces. We prefer to deduce $\mathcal{T}$ from the energy cost to make puddle edges.

We decompose the interfaces in three menisci. We will consider here one meniscus, and we will then add the contributions of the three menisci. The relevant geometry is described in Figure 2. The line is parallel to the y axis. The length measured along the line (curvilinear abscissa) is denoted s. The energy $\mathcal{E}_A$ of the line includes both a capillary term and a gravitational term. The profile to be determined is denoted $z = \zeta(x)$. We have

$$\mathcal{E}_A = \int_0^\infty \left[\gamma\left(\frac{ds}{dx} - 1\right) + \frac{1}{2}\rho g(e - \zeta)^2 \right] dx \tag{14}$$

where the first term represents the increase in surface area over the flat film and the second term describes the gravitational energy required to shape the film.

To find the profile $\zeta(x)$ that minimizes $\mathcal{E}_A$, we can write directly the equilibrium of the horizontal forces exerted on a slice of liquid (Figure 2). If α is the angle of the meridian tangent with the x axis,

$$\gamma(1 - \cos\alpha) - \frac{1}{2}\rho ge^2 + \int_0^{\zeta(x)} p(x, z)\,dz = 0 \tag{15}$$

where $p(x, z)$ is the hydrostatic pressure (excluding the atmospheric pressure p_0): $p(x, z) = \rho g(e - z)$.

Equation 15 simply reduces to

$$2\sin\left(\frac{\alpha}{2}\right) = \kappa(e - \zeta(x)) \tag{16}$$

The integral that gives the tension $\mathcal{E}_A$ (eq 14) then becomes

$$\mathcal{E}_A = \int_0^\infty dx \left(\frac{1}{\cos\alpha} - \cos\alpha \right) =$$
$$-\int_{\alpha_A}^0 2\sin\left(\frac{\alpha}{2}\right)\cos^2\left(\frac{\alpha}{2}\right)\gamma\kappa^{-1}\,d\alpha \tag{17}$$
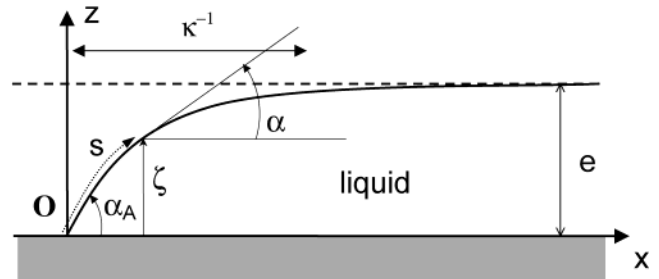
Figure 2. Geometrical parameters involved in the calculation of the line energy ($\mathcal{E}_A$) for one meniscus at the border of a liquid puddle (cross section).
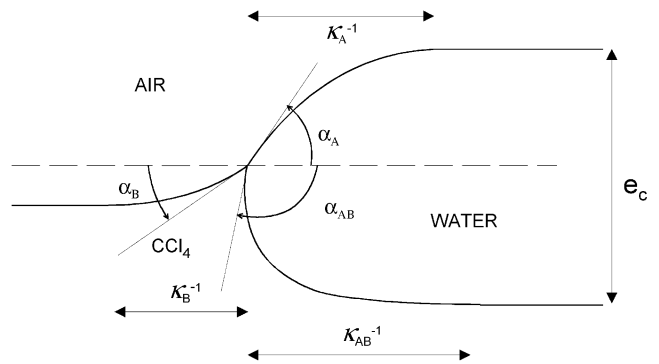
Figure 3. Border of a water puddle: schematic representation of the three menisci at the liquid/liquid/air contact line (cross section).

where we have introduced two successive changes of variable $dx = dz/\tan(\alpha)$ and $dz = -d\alpha\kappa^{-1}\cos(\alpha/2)$. The procedure yields

$$\mathcal{E}_A = \frac{4}{3}\gamma\kappa^{-1}\left(1 - \cos^3\left(\frac{\alpha_A}{2}\right)\right) \tag{18}$$

In the limit of small angles, eq 18 reduces to

$$\mathcal{E}_A = \frac{1}{2}\gamma\kappa^{-1}\alpha_A^2 \tag{19}$$

This holds for one meniscus.

In the liquid/liquid case, we have to add the three values for each meniscus, characterized by the three capillary lengths κ_A^{-1}, κ_{AB}^{-1}, and κ_B^{-1} and the three contact angles α_A, α_{AB}, and α_B shown in Figure 3. We have

$$\mathcal{T} = \mathcal{E}_A + \mathcal{E}_B + \mathcal{E}_{AB} \tag{20}$$

2.3. Energy of a Modulated Line. We consider now the contact line which borders the water puddle. We note $u(x)$ the deformation of the line with respect to the unperturbed position (straight line or arc of circle) and $u(q)$ the Fourier transform of the contour.

In the *capillary regime*, we can generalize the Joanny–de Gennes expression.

$$E_{el\,q} = \frac{1}{2}\tilde{\gamma}\theta_E^2|q||u_q|^2 \tag{21}$$

where $\tilde{\gamma}^{-1} = \gamma_A^{-1} + \gamma_B^{-1}$.[14,16]

In the *gravity regime*, deformations are screened at κ_{ij}^{-1}. The energy (as for a guitar string) is proportional to the increase of the contour length:

$$E_{el\,q} = \frac{1}{2}\mathcal{T}q^2|u_q|^2 \tag{22}$$

Table 1. Relevant Physical Constants for the System Water (A)/CCl₄ (B)

	γ_A	γ_B	γ_{AB}
interfacial tension (mN/m)	72.8	26.7	45

	ρ_A	ρ_B	$\tilde{\rho}$
volumic mass (kg/m³)	1000	1590	371

	κ_A^{-1}	κ_B^{-1}	κ_{AB}^{-1}
capillary length (mm)	2.72	1.31	2.79

$S = -91.1$ mN/m
$e_c = 7.08$ mm

with $\mathcal{T}$ given by eqs 18–20. Sekimoto et al.[21] give an expression which interpolates the two trends (in the small angle approximation):

$$E_{el} = \frac{1}{2}\tilde{\gamma}\theta^2 \int_{-\infty}^{\infty} dq\,(\sqrt{\kappa^2 + q^2} - \kappa)|u_q|^2 \quad (23)$$

In our studies, the angles are quite large and this expression is not exact. Nevertheless, in the gravity regime, studied here, we have an exact derivation of the line tension valid whatever the angles.

2.4. Experimental Determination of $\mathcal{T}$. Several techniques can be used to measure line tension $\mathcal{T}$. As for monolayers, one can measure $\mathcal{T}$ by following the relaxation of the contour of puddles distorted by electrical or mechanical forces.[20] We use here two static methods: (1) a classical technique proposed by Langmuir[14] and (2) a direct measure of the force exerted by the line on a vertical rod.

(a) Choice of the Two Liquids. We use deionized water deposited on carbon tetrachloride (CCl₄, 99.8%). In Table 1, we summarize the relevant physical parameters (from ref 22) for our system (A for water and B for CCl₄).

We have first studied the configuration of puddles of increasing volume V. From the measure of the radius R versus the volume V, we can deduce experimentally e_c, as first pointed out by Langmuir.[14] We deposit large drops of water on the substrate and form puddles. We have a relation (at first order in $1/R$) between the volume V of water and the radius R of the puddle:

$$\frac{V}{\pi R^2} \simeq e_c - \left(\frac{\Delta V}{\pi R} - \frac{e_c \mathcal{T}}{2|S|}\right)\frac{1}{R} \quad (24)$$

ΔV is the volume correction of the puddle compared to a cylinder of radius R and height e_c (which is proportional to R). Drawing $V/\pi R^2$ versus $1/R$, we determine $e_c = 7 \pm 0.1$ mm. We could also deduce $\mathcal{T}$ from the slope of the curve, but this method is not accurate because the major contribution comes from the volume correction. Thus, the measurement of $\mathcal{T}$ needs more refinement.

(b) Direct Measurement of the Line Tension. To measure directly $\mathcal{T}$, we first anchored the line on two points to make it straight. We used a rectangular (length, 26 cm; width, 10 cm; depth, 5 cm) glass container; half of the edges are covered by a Teflon strip not wettable by water. In this way, the contact line is straight and well anchored at rest. By using a metallic thin vertical rod, which anchors the line, we can pull or push the line and deform it. We can also use these rods as 2D defects, which pin the line. The rod is linked to a commercial strength sensor which gives the force f acting on the line (Figure 4). This force
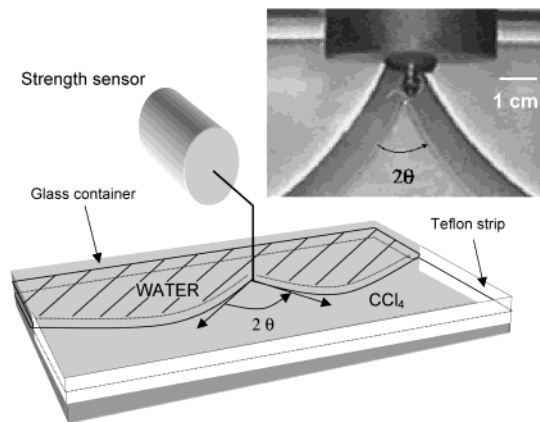
Figure 4. Experimental setup to measure line tensions. The line is anchored at the Teflon/glass boundary and exerts a force $f = 2\mathcal{T}\cos\theta$ on the strength sensor. The picture is a top view of the strength sensor and the line making an angle 2θ.
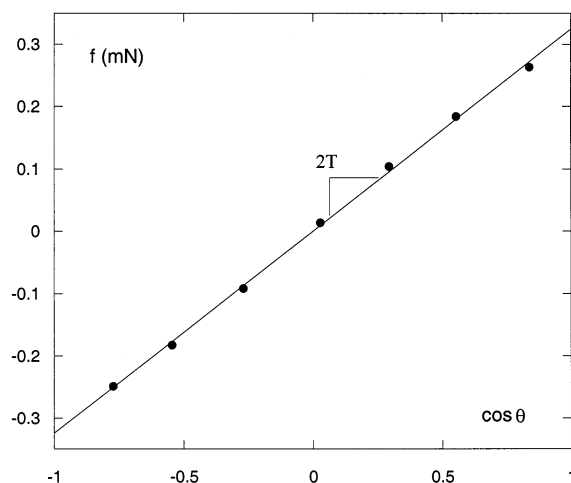
Figure 5. Plot of the force (f) acting on the line versus $\cos\theta$. 2θ is the angle made by the contact line stretched by the metallic rod coupled to the strength sensor. The slope is $2\mathcal{T}$.

is balanced by the line tension force: $f = 2\mathcal{T}\cos\theta$. By measuring f for different angles, we obtain the plot of f versus $\cos\theta$, shown in Figure 5.

We obtain a linear variation of the force versus $\cos\theta$. We noticed a slight deviation when θ tends to 0 or π: the line makes a kink (involving high q values where the gravity regime no longer applies). By measuring the slope of the straight line, we find $\mathcal{T} = 0.174 \pm 0.015$ mN. This value is lower than the calculated value: 0.20 ± 0.01 mN. [To calculate $\mathcal{T}$, we have to know the angles α_A, α_B, and α_{AB}. We did that by using (See ref 23) $2\gamma_{AB}\gamma_A\cos(\alpha_A - \alpha_{AB}) = \gamma_B^2 - \gamma_A^2 - \gamma_{AB}^2$ and eq 16, giving $2(\kappa_A^{-1}\sin(\alpha_A/2) + \kappa_B^{-1}\sin(\alpha_B/2)) = e_c(1 - \rho_A\rho_B)$ and $2(\kappa_A^{-1}\sin(\alpha_A/2) + \kappa_{AB}^{-1}\sin(\alpha_{AB}/2)) = e_c$. From eqs 18–20, we obtain a value of $\mathcal{T}$ for the water/CCl₄ system: $\mathcal{T} = 0.20 \pm 0.01$ mN, where the error bar comes from the uncertainty on the surface tension values.] Impurities can modify surface energies and decrease the line tension. This may explain the slight difference.

3. Dynamics of Triplons

We study now the oscillations of the triple line at wavelengths larger than the capillary length. In this regime, the elasticity of the line is described by the line tension $\mathcal{T}$.

(20) Benvegnu, D. J.; McConnell, H. M. *J. Phys. Chem.* **1992**, *96*, 6820–6824.

(21) Sekimoto, K.; Oguma, R.; Kawasaki, K. *Ann. Phys.* **1987**, *176*, 359–392.

(22) Israelachvili, J. N. *Intermolecular and Surface Forces*, 2nd ed.; Academic Press: London, 1985.

(23) Noblin, X. Rapport de stage de DEA de Physique des Liquides, Université Paris 6, 2000.
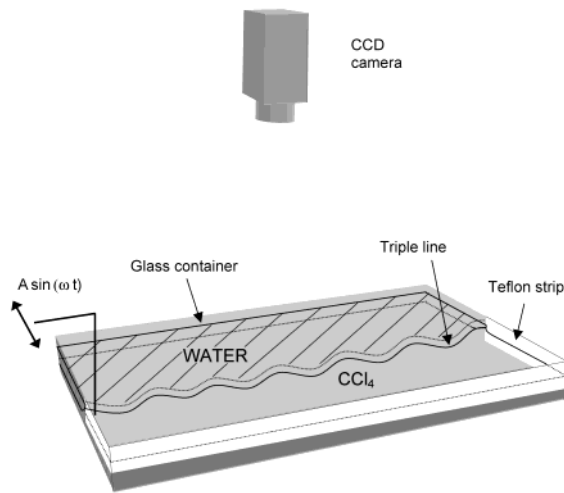
Figure 6. Experimental setup to measure the dispersion relation of triple line waves. The line is anchored to one end at the Teflon/glass boundary. At the other end, a metallic rod gives to the line a sinusoidal motion, which propagates along the liquid/liquid/air contact line.
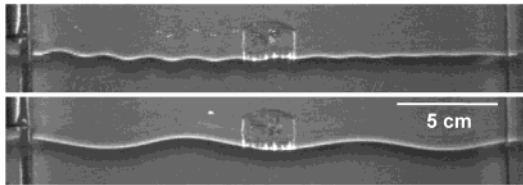
Figure 7. Pictures of triple line waves at the border of a water puddle lying on a CCl_4 substrate. Top: $f = 4.6$ Hz; the viscous decay length is small compared to the container size, and reflected waves are negligible. Bottom: $f = 0.5$ Hz; stationary waves patterns allow us to measure the wavelengths as a function of frequency.

3.1. Observations. We used the same container as for static measurements and the same method to have a straight line at rest. We anchored one end of the line on a metallic rod linked to the moving part of a tracing table. The motion is sinusoidal ($u_0 \sin(\omega t)$), with the amplitude (u_0) ranging from 1 to 5 mm and the frequency (ω) ranging from 1.5 to 60 rad·s^{-1} (0.25 to 10 Hz). The modulations of the line are recorded by a CCD camera placed above the container (Figure 6). Frequency was measured by looking at the movement of the rod on video images (25 or 50 images per second). The error is of the order of 0.5%. The contact line can be easily observed because of strong refraction of light in the menisci zone. The curvature of fluid interfaces, by a "lens effect", induces a strong local change in intensity and allows us to measure the wavelength of the waves.

Viscous attenuation of the waves is clearly observed but the change of the relation between frequency and wavevector (propagative part) is not significant in the explored regime. If we note a the viscous attenuation decay length, we have $a/\lambda \simeq 10$. When waves reach the end of the container, they are reflected and interfere. Due to partial reflection and viscous attenuation, to characterize the wave pattern, we must include r (the amplitude−reflection coefficient) and a.

When a is smaller than the container lentgh (L), reflected waves do not contribute to the total amplitude, and we can measure the wavelength directly by observing the undulations. In Figure 7 (top), we can assume that reflected waves have negligible effects for measuring the wavelength.

When a becomes of order L, we cannot neglect reflected waves. Then, one way to measure the wavelength is to
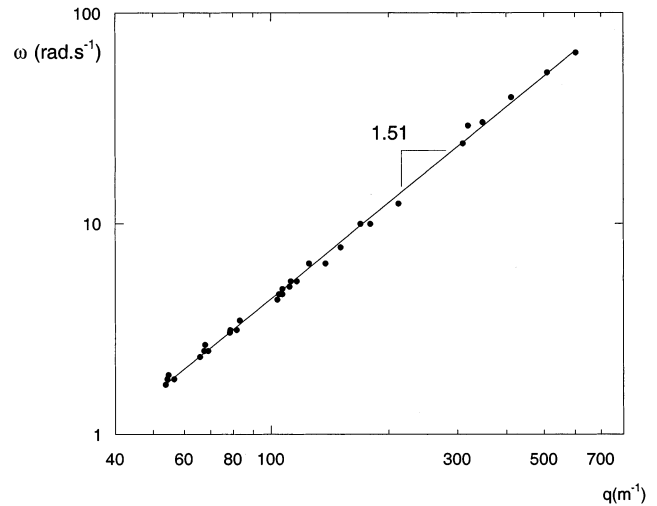
Figure 8. Plot of the excitation angular frequencies (ω) versus wavevector (q) for the triple line waves (triplons) of a water puddle floating on a CCl_4 substrate. We find $\omega \propto q^{1.51}$.

look at the line just after the beginning of excitation and before the wave reflection (transient period).

When a becomes larger than L (for slow modes, $\lambda \simeq 5 \rightarrow 12$ cm), we can use stationary waves to measure λ: the goal is to find, for different spatial modes, the frequency where we reach standing wave conditions (for a line anchored at one end, it is given by $L = (2n + 1)(\lambda/4)$). The wave pattern cannot be completely stationary because of dissipation and partial reflection, but we can find the frequency where this condition is the best defined (Figure 7 (bottom)). By looking at the wave pattern when the amplitude is maximum, we can measure directly the wavelength.

Values obtained by stationary conditions and direct values are in good agreement. On a log−log plot the experimental points (Figure 8) give $\omega \propto q^{1.51}$. The exponent is very close to 3/2.

We noticed that the excitation of triplons for frequencies higher than about 10 Hz is more difficult, because the moving rod can induce surface waves on the two fluids which are coupled to line waves. We cannot observe the modes localized at the triple line anymore.

We have also excited the line waves with a completly different setup. We performed electrostatic excitation with an electrode close to the line at high voltage (of order 2 kV) in the same frequency range. The shape of the electrode has to be optimized to induce line waves and not surface waves. We observed that the ratio between the line wave amplitude and the surface wave amplitude seems to decrease as frequency increases. For low frequencies (less than 1 Hz), triplons are strongly dominant. The advantage of this technique is that it allows easy exploration of the regime of short wavelengths, but as frequency increases, surface waves show up.

3.2. Interpretation. We derive here the general structure of the dispersion relation from a global force equation for the motion of the contact line, ignoring numerical coefficients. An exact calculation, with a full description of the flow field is given in the appendix. The deformation, for a mode of wavevector q, can be written as $u = u_q e^{i\omega t} e^{iqx}$. The modes observed propagate and are governed by a balance between inertial, elastic, and viscous forces:

$$-\mathscr{T}q^2 u = M\ddot{u} - f_V \tag{25}$$

where M is the mass of liquid put into motion, $\ddot{u}$ is the acceleration, and f_V is a friction force associated with the

viscous dissipation in both liquids. We now discuss M to derive the dispersion relation in the inertial regime and f_V, which controls the damping of the modes.

(a) Mass M of Triplons. To estimate M, we assume that the floating liquid behaves like an incompressible monolayer of thickness e_c on the water side and thickness $e' = \rho_A e_c / \rho_B$ on the CCl_4 side. The 2D plug flows, as shown in the appendix, are screened out at a distance q^{-1}. Below the A/B interface, the velocity field induced by the triplons at frequency ω penetrates within a thickness $h_\omega = (\eta_B/\rho_B\omega)^{1/2}$. h_ω is the boundary layer thickness. An essential parameter is the ratio h_ω/e_c. The inertial regime studied here corresponds to $h_\omega \ll e_c$. When $h_\omega > e_c$, we enter in the viscoinertial regime where the real and imaginary parts of ω_q are comparable.[5] Another parameter is the depth H of the B liquid bath. If $h_\omega/H > 1$, we enter in the "shallow" regime, and $h_\omega = H$ (the flows are simple shear flows). To summarize, $M = 2\rho_A(e_c + h_\omega)q^{-1}$.

For the *inviscid mode*, neglecting f_V in eq 25 and assuming $h_\omega \ll e_c$, we obtain the dispersion relation

$$\omega^2 = \frac{1}{2}\frac{\mathcal{T}q^3}{\rho_A e_c} \qquad (26)$$

where we have included the numerical coefficient derived in the appendix.

(b) Damping of the Inertial Modes = Discussion of f_V. The friction force f_V is the sum of the friction associated (i) with the plug flow in the upper layer $f_{Vu} = (\eta e + \eta_B e')qu$ and (ii) with the vorticity flows induced in the B bath $f_{Vb} = \eta_B u q^{-1}/h\omega$. For the long wavelengths studied here, $f_{Vu} \ll f_{Vb}$ and we can assume that $f_V \simeq \eta_B u/(qh_\omega)$.

(c) Dispersion Relation. (i) *Thin Bath*: $h_\omega = H$. In this limit, eq 25 can be written as

$$\frac{\mathcal{T}q^3}{\rho_A e} = \omega^2 - i\omega\omega_1 \qquad (27)$$

where $\omega_1 = \eta_B/H\rho_A e$.

For $\omega \gg \omega_1$, we have a propagative mode of wave vector

$$q = q_0(\omega)\left(1 - \frac{i}{3}\frac{\omega_1}{\omega}\right) \qquad (28)$$

where $q_0(\omega)$ is the solution of eq 26 for inviscid liquids.

The oscillation of the rod $u = u_0 e^{i\omega t}$ induces an undulation of the contour: $u = u_0 e^{iq_0(\omega)x}e^{-x/a}$, which propagates up to a distance a along the line with $aq_0 = \omega/\omega_1$.

Remark 1: If $\omega < \omega_1$, the mode is damped (viscous regime): $i\omega = -\mathcal{T}q^3 H/\eta_B$.

(ii) Thick bath: $h_\omega \propto \omega^{-1/2} < H$. In this limit, eq 25 becomes

$$\frac{\mathcal{T}q^3}{\rho_A e} = \omega^2 - i\omega^{3/2}\frac{\eta_B^{1/2}\rho_B^{1/2}}{\rho_A e} = \omega^2\left(1 - i\left(\frac{\omega_2}{\omega}\right)^{1/2}\right) \quad (29)$$

where $\omega_2 = (\eta_B\rho_B)/(\rho^2 e^2)$. The complex wavevector solution of eq 29 is

$$q = q_0(\omega)\left(1 - \frac{i}{3}\left(\frac{\omega_2}{\omega}\right)^{1/2}\right) \qquad (30)$$

The length a of damping is given now by $aq_0 = (\omega/\omega_2)^{1/2}$.

Remark 2: If $\omega < \omega_2$, we expect a viscoinertial regime

$$\frac{1}{\mathcal{T}_q} \propto \frac{\mathcal{T}^{2/3}q^2}{\rho_B^{1/3}\eta_B^{1/3}}(1 + i)$$

3.3. Discussion. *(1) Dispersion Relation of gravity Triplons.* We have observed propagating triplons with water floating on a thick CCl_4 bath. This is in agreement with our predictions, because our frequency range (0.25−10 Hz) is always larger than $\omega_2 = 510^{-3}$ Hz, calculated from eq 29. The dispersion relation determined experimentally is

$$\omega = k\sqrt{\frac{\mathcal{T}}{2\rho_A e_c}}q^{1.51\pm0.05} \qquad (31)$$

where $k = 1.09$ instead of 1.

This result is compatible with our model. The ratio ω/ω_2 gives the number of wavelengths which can be observed before damping. It is in qualitative good agreement with our observations.

(2) Gravity versus Capillarity. In the limit $q > \kappa$ (capillary regime), the elasticity of the line is anomalous and described by eq 21. The balance between elastic and inertial forces becomes

$$-\tilde{\gamma}\theta_E^2 qu = M(q)\ddot{u} \qquad (32)$$

The mass of liquid put into motion is now $M \sim \rho q^{-2}\theta_E$. Equation 32 leads to the dispersion relation in the capillary regime

$$\omega \approx \sqrt{\frac{\tilde{\gamma}\theta_E}{\rho}}q^{3/2} \qquad (33)$$

Thus, surprisingly, the scaling law ($\omega \sim q^{3/2}$) is the same in the gravity and the capillary regimes, but the numerical coefficient is different.

Remark: We expect that this result is also valid for triple lines at the edge of a liquid puddle on a solid substrate. In ref 6, the prediction for inertial triplons was $\omega \sim q^{3/2}$ in the capillary regime and $\omega \sim q$ in the gravity regime. The flow was assumed to be screened out over a length κ^{-1}. This was wrong. In fact, a modulation of the surface pressure penetrates the liquid puddle on a scale q^{-1}, because the plug flows (on a solid or a liquid bath) are all described by eq 36 (Appendix 1). This correction may help to explain recent results with superfluid helium showing that triplons are dispersive even at wavelengths larger than κ^{-1}.[13]

(c) Triplons versus Capillary Waves. At low frequencies, we have observed one-dimensional modes of the triple line. At high frequencies, they seem to be coupled to the classical two-dimensional surface waves. We can understand this by the following argument. In the gravity regime, the surface waves obey the dispersion relation $\omega = (gq)^{1/2}$. A vibration of the driving rod at frequency ω couples to 1D waves of wave vector q_0 and may also induce 2D waves of wave vector $q_s \sim q_0(q_0/\kappa)^2$. As long as $q_0 \ll \kappa$, that is, in the gravity regime studied here, these waves are well decoupled. But when $q_0 \sim \kappa$, a large mixing takes place. To reduce this effect, one should use more wettable liquids ($e_c \ll \kappa^{-1}$). In this limit, the capillary triplon (q_0) and surface ripple (q_s) wave vectors should remain distinct ($q_s \sim q_{0o}\theta_E^{3/2}$).

4. Concluding Remarks

A liquid substrate is free of defects and free of hysteresis. It allows for complete studies of both static and dynamic contact lines. A liquid puddle is limited by minimal lines (arcs of circles). There is a 2D Laplace pressure—a small puddle flows into a larger one, when they are put into
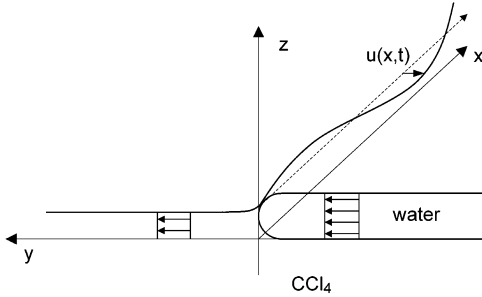
Figure 9. 2D velocity profile of flows in the puddle (plug flows) and in the substrate induced by triplons.

contact—stretched by an external force, the deformation of the contour allows a direct measure of the line tension $\mathcal{T}$.

For the dynamics, we have been able to follow the vibrations of a triple line. Wavelengths up to several centimeters have been observed. These gravity/inertial modes were not accessible on a solid substrate—even on a silanized silicon wafer—because their energy becomes extremely small, and the line is easily pinned by weak defects on the substrate.

We have shown that long wavelength gravity triplons obey the same scaling relation as short wavelength capillary triplons. "Capillary" triplons, predicted theoretically in ref 4, have been observed recently on a solid substrate with superfluid helium.[13] The interpretation is the following: for gravity mode (rope elasticity), the force $\mathcal{T}q^2u$ is balanced by $M\omega^2u$, with $M \sim e_c q^{-1}\rho$. For capillary modes (fringe elasticity) the force γqu is balanced by $M\omega^2u$, with $M \sim \theta_E q^{-2}\rho$. By some sort of coincidence, the two laws look the same, although they are related to different physical processes.

Appendix 1: Complete Description of Inertial Triplons

We derive here the flow field and the surface pressure in the film induced by the deformation of the line. We consider inviscid fluids with plug flows (Figure 9). The modulation of the line gives rise to a surface pressure difference between the A film and the bare substrate

$$\Pi_{A0} - \Pi_{B0} = -\mathcal{T}\frac{\partial^2 u}{\partial x^2} \qquad (34)$$

The gradient of surface pressure generates 2D planar flows v_p ruled by a 2D Euler equation:

$$\rho e \frac{\partial \vec{v}_p}{\partial t} = -\vec{\nabla}_p\Pi \qquad (35)$$

where $\rho e = \rho_A e_c = \rho_B e'$. We look for sinusoidal modes written as

$$\Pi = \Pi(y)e^{i(\omega t - qx)}$$

$$\vec{v}_p = \vec{v}_p(y)e^{i(\omega t - qx)} \qquad (36)$$

$$u = u_0 e^{i(\omega t - qx)}$$

Notice that eqs 34−36 will also describe capillary waves at a liquid A/liquid B interface in zero gravity, with an effective interfacial tension $\gamma_{AB} = \mathcal{T}/e_c$.

Equation 35 becomes

$$\vec{v}_p = -\frac{\vec{\nabla}_p\Pi}{i\omega\rho e} \qquad (37)$$

We assume that the film is uncompressible. This is correct if the triplons' modes are slow compared to the peristaltic modes in the film discussed in Appendix 2. $\text{div}(\vec{v}_p) = 0$ leads to

$$\Delta\Pi_s = 0 \quad \text{then} \quad \frac{\partial^2\Pi_s}{\partial y^2} - q^2\Pi_s = 0 \qquad (38)$$

The solution is on side A ($y < 0$) $\Pi_s = \Pi_{A0}e^{qy}$, which tends to zero far away from the line. On the side B ($y > 0$) $\Pi_s = \Pi_{B0}e^{-qy}$

Equation 34 gives

$$\Pi_{A0} - \Pi_{B0} = \mathcal{T}q^2 u_0 \qquad (39)$$

We can calculate v_y at both sides of the contact line

$$v_y(y=0) = -\frac{1}{i\omega\rho e}\frac{d\Pi}{dy}\Big|_{y=0} = -\frac{q\Pi_{A0}}{i\omega\rho e} = \frac{q\Pi_{B0}}{i\omega\rho e} \qquad (40)$$

It gives $\Pi_{A0} = -\Pi_{B0} = \frac{1}{2}\mathcal{T}q^2 u_0$. With $v_y = i\omega u$, we get

$$\omega^2 = \frac{1}{2}\frac{\mathcal{T}}{\rho e}q^3 \qquad (41)$$

Appendix 2: Peristaltic Modes of the Floating A Liquid

We have seen that the effective film surface tension is $\tilde{\gamma}_B = \gamma_{AB} + \gamma_A - \frac{1}{2}\tilde{\rho}ge^2$. At equilibrium, $e = e_c$ and $\tilde{\gamma}_B = \gamma_B$. If e is modulated around e_c, $e = e_c + \alpha e^{iqy}e^{i\omega t}$, the surface pressure oscillates, and flows are induced in the film.

$$\rho_e\frac{\partial\vec{v}_p}{\partial t} = -\vec{\nabla}_p\Pi = \rho g e_c \vec{\nabla}_p e \qquad (42)$$

With the volume conservation

$$\frac{\partial e}{\partial t} + \text{div}(ev) = 0 \qquad (43)$$

we get

$$\omega = \pm\sqrt{egq} \qquad (44)$$

The modes propagate at velocities $(ge)^{1/2} \simeq 26$ cm/s. These velocities are much larger than $v_\rho = q^{1/2}(\mathcal{T}/2\rho e)^{1/2}$ (in our experiments, 3 cm/s $< v_\rho <$ 10 cm/s. We can thus consider the film as uncompressible.